scientific reports

Check for updates

OPEN

Experimental investigations on hybrid manufacturing: WEDM of WAAM-fabricated stainless-steel components using ANFIS modelling

P. Thejasree[1], N. Manikandan[1], Siva Marimuthu[2], Rajadurai Murugesan[3], D. Palanisamy[4], Mukesh Kumar[5], Arun Kumar[6] & Regasa Yadeta Sembeta[7]✉

Wire Arc Additive Manufacturing (WAAM) enables the fabrication of large, near-net-shape stainless steel components, but the resulting surfaces require precision post-processing to meet industrial standards. In this study, Wire Electrical Discharge Machining (WEDM) was applied as a finishing process for WAAM-fabricated SS316L components, and a hybrid optimization–prediction framework was developed using Taguchi design, Grey Relational Analysis (GRA), and Adaptive Neuro-Fuzzy Inference System (ANFIS) modeling. In total, there were 27 experimental runs conducted at different pulse-on, pulse-off, and current conditions. The results showed that pulse-on time (T_{on}) was the dominant influencing factor in the case of material removal rate (MRR), dimensional deviation (DD), and GD&T errors, while pulse-off time (T_{off}) was significantly regulated to surface roughness (SR) and geometric stability. The experimental analysis revealed that pulse-on time (T_{on}) was the most influential parameter governing material removal, dimensional accuracy, and geometric errors, whereas pulse-off time (T_{off}) played a key role in controlling surface finish and geometric stability. This emphasizes the critical importance of discharge control for achieving high-quality post-processing of WAAM components. For multi-response optimization, GRA provided a composite performance index that was used to train the ANFIS model. The predictive outcomes exhibited excellent agreement with experiments, confirmed by very low error metrics (MAPE = 2.19%, RMSE = 0.027, MAE = 0.022) and a strong correlation (R^2 = 0.9985). Overall, the WAAM–WEDM hybrid framework not only improves surface quality and dimensional consistency but also establishes a scalable, intelligent manufacturing pathway with strong potential for aerospace, biomedical, and energy applications.

Keywords Hybrid manufacturing, SS316L, Wire arc additive manufacturing (WAAM), Wire electrical discharge machining (WEDM), Adaptive neuro fuzzy inference system (ANFIS)

Additive Manufacturing (AM) is rather known by different terms named as layer manufacturing or generative manufacturing, rapid prototyping, desktop manufacturing, and digital manufacturing, all started in the 1980's and have been under a constant evolution until now. WEDM is a well-acknowledged finishing technique employed for WAAM manufactured parts. Apart from parting them into structure, it is used for surface improvement and dimensional accurateness besides WAAM alloys[1–6]. AM fabricates extremely customized and sophisticated parts by adding them layer by layer, yielding manifold advantages over conventional production methods including

[1]Department of Mechanical Engineering, School of Engineering, Mohan Babu University, Tirupati, Andhra Pradesh 517102, India. [2]Department of Engineering, Stoke on Trent, University of Staffordshire, Stoke-on-Trent, UK. [3]Department of Aeronautical Engineering, Nitte Meenakshi Institute of Technology, Bengaluru, India. [4]Department of Mechanical Engineering, Adhi College of Engineering and Technology, Kancheepuram, Tamil Nadu, India. [5]Department of Mechanical Engineering, Mewar University, Chittorgarh, Rajasthan, India. [6]Center for Promotion of Research, Graphic Era (Deemed to be University), Dehradun, Uttarakhand 248001, India. [7]Department of Civil Engineering, College of Engineering and Technology, Mattu University, Metu 318, Ethiopia. ✉email: yadetaregasa@gmail.com

elimination of complex supply chains, minimal wastage of materials, low tooling requirements, shorter production lead times and reduced process time as a result of compressed design cycles or minimal design iteration before releasing for fabrication[7–13].

The inbuilt direct approach and its output correlation significantly reduce total energy consumption, while also decreasing carbon emissions and greenhouse gas outputs, making additive manufacturing (AM) a potential green manufacturing technology. While AM has been viewed as a supplement to industrial manufacturing, it has now expanded application areas far beyond conventional processes, emphasising the transformative capability of modern production systems[14–22]. Thus, there are very wide ranges of AM methods available commercially. Various researchers have differed in proposing different classification schemes for AM technologies based on its working principles as well as applications[3,8,23–25]. Among these categories, Direct Energy Deposition (DED) is the most prominent method for effectively manufacturing components that requires significantly higher energy inputl2. Figure 1 shows a schematic of a general DED setup.

The heating causes a melted spot on-site, which permits the depositing of the filler material in the shape of wire, powder, or both[26–28]. Because rapid solidification of the molten pool occurs when the heat source moves away from the deposition point, a structure can be formed layer by layer[29,30]. The DED method consists of advantages such as increased deposition rates compared with Powder Bed Fusion (PBF), repair of existing components, and flexibility in fabrication of functionally graded materials[31–34]. Limitations to DED include the need for supports and that it provides relatively poor surface finish when compared with other AM processes[35–39].

Although WAAM allows the rapid manufacture of large, near-net-shaped metallic components, it usually leads to poor surface finish, dimensional inaccuracies, and residual stresses. Wire Electrical Discharge Machining (WEDM) comes in as a cost-effective post-processing technique mainly focused on As-Welded or in-the-raw materials of titanium alloy, Inconel, stainless steels among others for WAAM. WEDM enhances surface finish while maintaining tight tolerances and avoiding damage to the microstructure. It, therefore, acts as a total complementary operation to WAAM in terms of producing top-end components for aerospace and biomedical applications[40–45].

In the non-traditional machining genre of Wire EDM, material removal occurs through a continuous of discrete electrical discharges interspersed amongst a continuously moving wire electrode and an electrically conductive work material sunken in a dielectric medium. The process is suitable for intricate profiles, high-precision machining, and harder materials that are hard to machine conventionally. WEDM, in particular, ensures tighter tolerances and a better surface finish to WAAM-fabricated components[46–48]. Among many advantages for steel, WAAM offers an efficient method to fabricate complex structures, thus enhancing material properties therein and is deployed across energy, automotive, aerospace, and construction applications. Controlling certain critical process variables during WAAM is required to minimize defects and realize desirable microstructure and mechanical properties. Good process design thus relies on computational modelling aided by optimization through AI. Given the challenges of porosity and residual stresses, WAAM handles the interesting dilemma of being flexible, sustainable, and high-potential for the production of large-scale, complex steel components[49–52].

EDM and machining have been previously studied from many angles including the micro-impression making on Al6061, process optimization from sustainability standpoints, performance of machining with economic and environmental analyses[3], predictive modelling via ANN, optimization of complex features, parametric and multi-objective optimization, enhancement of high-speed cutting of EDM performance[10], and micro-machining

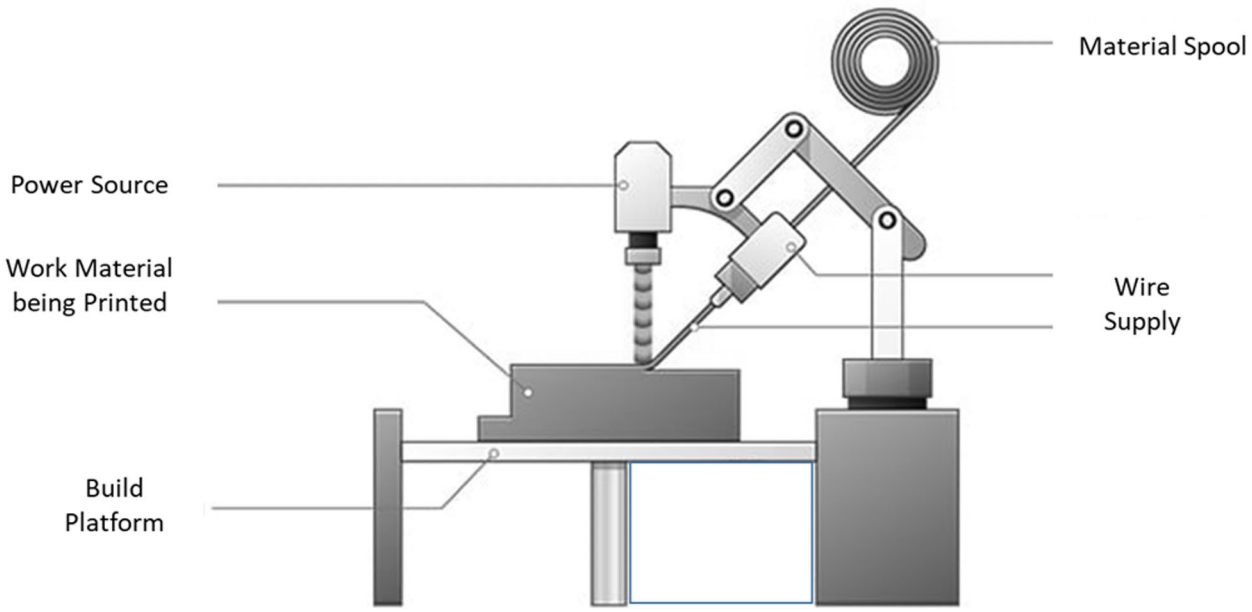

Fig. 1. Schematic of DED method.

error reduction. While these works present some surface finishing, economic and environmental metrics, and some error reduction on machining, they usually concern single-objective optimization or specific materials. In contrast, the present study examines hybrid WAAM-WEDM components, which are challenged greatly by layer-induced anisotropy and recast layer formation. Taguchi-TOPSIS experimental design integrates with ANFIS-based multi-objective prediction in optimizing material removal rate, surface roughness, and dimensional accuracy simultaneously. The hybrid experimental-predictive strategy describes a more integrated view of process performance, overcoming gaps toward sustainability, accuracy, and multi-objectives optimization for advanced manufacturing applications[41,53–56].

Unlike the conventional finishing methods such as CNC milling and laser-based machining, WAAM-WEDM gives better benefits than these finishing technologies. CNC milling is a very precise technology, but machining near-net-shape WAAM components does not offer the full potential of this machining due to the common access limitations shown by the tool on the surface of the workpiece together with residual stresses and tool wear in highly hardened or irregular geometries. Laser polishing and other laser-based finishing methods can improve surface smoothness, but this may be at the expense of producing thermal distortion, localized melting, and microstructural changes, particularly in stainless steel alloys. Unlike these processes, WEDM offers an ideal non-contact, thermal-electrical removal mechanism that is very suitable for complicated components manufactured through WAAM, allowing for high precision in dimensional controls, low mechanical stresses, as well as a fine surface finish, without leading to a large tool wear. These advantages of WAAM-WEDM thus make it a truly versatile and dependable finishing method for such complex additively manufactured parts with applications in aerospace, biomedical, and energy sectors. From the perspective of sustainability, the WAAM-WEDM hybrid method has huge benefits in terms of cost and energy against all the conventional methods currently in use. WAAM processes nearly net shapes, and WEDM utilizes very low wear and fine remoteness finishing without resourcefulness. The hybrid approach uses generally less time and costly tool replacements in comparison with CNC milling, thereby reducing energy input and operational expenditure as sustainable for high-performance components in aerospace and energy applications[42].

Combinations of hybrid WAAM and WEDM have some intolerable complexities for the quality and performance of a component. Besides other things, the WAAM surfaces were found to be often rough, porous, and micro-cracked, which further worsens recast layers produced during WEDM operation, deteriorating surface integrity and mechanical properties. Layer-by-layer deposition leads to anisotropic microstructures, resulting in directional variation in properties such as strength and ductility, while thermal gradients create residual stresses, predisposing them to distortion or dimensional inaccuracy. Completion of such hybridization is complicated because many interacting factors concerning material properties, deposition strategy, and machining parameters come into play and thus have to be modelled and predicted further to create consistent high-quality processes.

It is observed in existing literature that WAAM is an additive process that is recognised for producing highly efficient deposition rates and cost-effective, large-scale, nearly net-shaped metallic components. Among various materials suggested for WAAM, steel and steel alloys appear to be the most commonly used due to their mechanical strength and availability. However, the parts produced by a WAAM typically suffer from some inherent limitations, such as poor surface finish and dimensional inaccuracy that totally restrict their applicability in precision-critical applications. WEDM is an alternative method that has been proposed in that it is non-contact-based and uses thermal erosion, which allows the precision finishing of WAAM parts. In addition, WEDM ensures machining of high-strength steels and has the capability of processing complicated geometries with high accuracy and little residual stress after WEDM. It is essential to understand how WEDM variables impact various dependent metrics, such as material removal rate, surface roughness, dimensional deviation, and GD&T errors (parallelism error, perpendicularity error). This understanding reveals the exclusive investigational analysis and evolution of the hybrid WAAM-WEDM framework, confirming high-quality post-processing of steel components.

Materials and methods

This study focuses on SS316L, a low-carbon austenitic stainless steel known for its exceptional resistance to corrosion, high strength, and superior weldability. Because of these amazing qualities, SS316L is often used in aerospace applications such as aircraft wing parts, where a high strength-to-weight ratio and the ability to last in extreme conditions are very important. Its reliability and performance also make it suitable for critical engineering applications in marine, biomedical, and chemical processing, where material integrity over extended service life is essential. The chemical composition of base metals is delineated in Table 1.

For this experimentation, a Wire Electrical Discharge Machining (WEDM) setup (Model: DK 7732, Concord make) equipped with a molybdenum wire electrode was utilized. The experimentation setup is illustrated in Fig. 2. Through all experiments of WEDM kept continuously controlled spark generation with the effective removal of debris by deionised water-based dielectric fluid. The dielectric was then filtered through fine filtration to remove the machining debris, which could otherwise alter the conductivity of the dielectric medium in the range of 10–20 µS/cm. Throughout the experiment, the temperature of the dielectric was maintained at 25 ± 2 °C to ensure thermal consistency and avoid unwelcomed variations in discharge characteristics. Clear checks

Base Materials	Fe	*P*	C	Mo	Si	*N*	Ni	Cu	Mn	Cr	S
SS316L	Bal.	0.028	0.025	2.03	0.38	0.037	10	0.16	0.16	16.55	0.027

Table 1. Chemical Composition of base material (wt%).

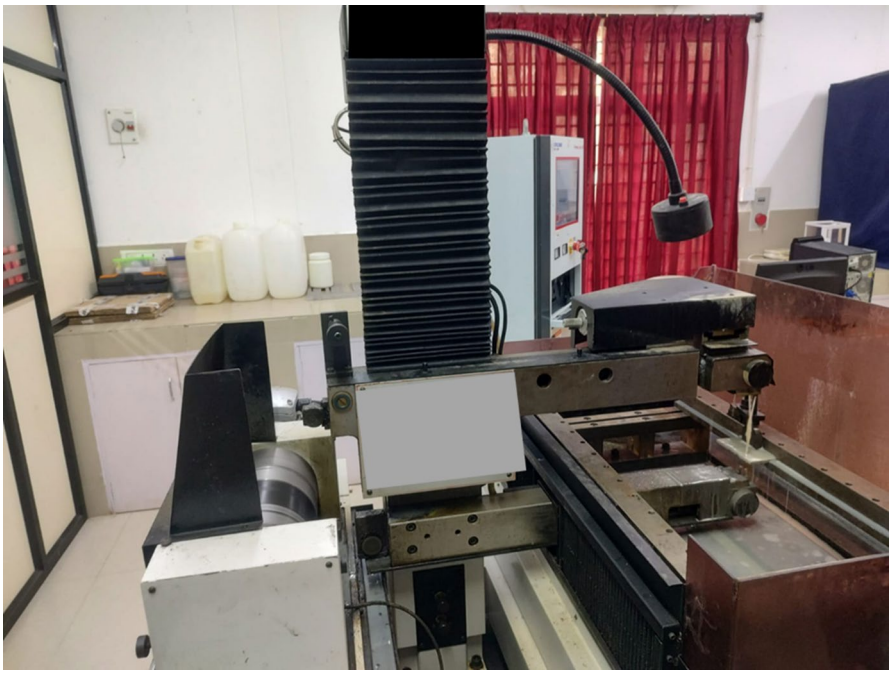

Fig. 2. Experimental Setup (WEDM for Machining).

Symbols	Factors	Levels		
		1	2	3
A	'T_{on}' (µs)	30	35	40
B	'T_{off}' (µs)	5	10	15
C	Peak Current - (A)	2	3	4

Table 2. WEDM variables and their levels.

were done to maintain fluid clarity and conductivity before every experimental run. With all these measures, uniform quality of dielectric was assured with stable machining condition that, in turn, aided in uniform erosion behaviour and preservation of surface integrity of WAAM-fabricated SS316L specimens.

The selected output responses include Material Removal Rate (MRR), Surface Roughness (SR), Dimensional Deviation (DD), and orientation tolerance. The work piece was machined into a square-shaped hole. MRR was determined based on the weight loss approach, using a 'Contech' digital weight balance with a precision of 0.0001 g. Roughness of the machined surface was evaluated by a contact-type tester (Make: Mitutoyo, Model: Surftest SJ-310). Orientation error was assessed using a Coordinate Measuring Machine (CMM – Made by Helmel). Each of the three triplicates for this investigation contained all experimental work. For each parameter under investigation, three independent trials were conducted under the same conditions, and the average was considered for analysis.

The present explorative analysis examines the influence of three independent process factors: pulse duration (on/off time in µs), and peak current (A). The specific levels for each of these variables are detailed in Table 2. To evaluate the significance and interaction of these factors across multiple levels, a structured set of experiments was essential. The Taguchi method here comes very handy for optimizing the process variables and lessening in experimental effort. The factors selected, with their levels, are based on the use of the L27 Orthogonal Array (OA), thus allowing a systematic and good analysis of the influence of process factors on the output responses.

The SS316L material examined in this study was fabricated utilising WAAM Technology. The WAAM technique is a Directed Energy Deposition (DED) method capable of producing near-net-shape metallic parts. Parts manufactured by this technology are based on a layer-wise method whereby electric arc current acts as a source of heat, while metallic wire serves as feedstock. The deposition was carried out under controlled conditions to achieve metallurgical consistency and reduced oxidation. The SS316L samples thus fabricated became the subjects of the experimental investigations, especially in the tests for machinability and surface characteristics using a WEDM method. The use of WAAM-fabricated material enhances the relevance of this work to the analysis on the performance of additively manufactured stainless steel for precision machining applications.

SS316L specimens were fabricated using a TIG-based WAAM setup (DED, GTAW system) with 1.2 mm SS316L wire and high-purity argon shielding (15–18 L/min). Process parameters included 110–130 A (DCEN),

18–22 V, a deposition rate of 2.5–3.0 kg/h, and a travel speed of 200–250 mm/min. Layers averaged 1.5–2.0 mm thickness, with interlayer temperatures controlled at 150–200 °C. The final build was a 100 mm × 50 mm × 10 mm rectangular block for WEDM trials.

Results and discussions

These experimentations have been done in continuation with L27 OA and now the results are used to evaluate the importance of the input factors in the WEDM process of SS316L manufactured by WAAM. A systematic effort has been made to identify the critical parameters necessary for developing a proficient and effective WEDM process. Different output variables are thus reflected in this exploratory study, which is designed to introduce variations regarding the possible effect of process factors in the WEDM process. The favourable performance measures included maximum material-reduction ratio, minimum roughness, variation in dimension and form/orientation error.

Ascendency of variables on MRR

In WEDM, for WAAM components made of SS316L, the MRR increased significantly with a rise in the pulse-on time (T_{on}) and applied current. This behaviour can be attributed to an increase in thermal energy and discharge characteristics. As shown in Fig. 3, if the pulse-on duration is increased, there is a greater interval provided for energy transfer per electrical discharge, and this results in larger craters formed on the work piece surface due to more localized melting and vaporization. Therefore, this increases the rate of material erosion. Meanwhile, more extended pulse-off time (T_{off}) will ensure adequate dielectric recovery and efficient debris removal from the spark gap. This is crucial for WAAM-made designs, characterized by inter-layer porosity and surface roughness, since an efficient dielectric recovery guarantees a sustained spark and, hence, effective machining.

An increase in applied current also increases the discharge energy per pulse, resulting in higher localized temperature and hence more aggressive material removal. The specific features of WAAM-formed SS316L, such as its layered microstructure, possible anisotropy, and variation in thermal conductivity, also involve the heat-affected zone and the dynamics of spark propagation, making the material much more susceptible to mechanisms of thermal erosion. Ultimately, all the above factors help in making the trend MRR increase with an increase in 'T_{on},' 'T_{off},' and current and establish the interrelationship between electrical parameters and metallurgical properties in additively manufactured SS316L.

Collectively, these factors result in a noticeable rise in MRR with increased values of pulse duration and peak current during WEDM of WAAM-fabricated SS316L. It is noticed that the optimal variable combinations for attaining enhanced MRR is $A_3B_3C_3$ which means higher levels of process variables.

Ascendency of variables on SR

Figure 4 reflects the influence of WEDM process parameters on surface roughness (SR). With increasing values of pulse-on time (T_{on}) and applied current, the degree of surface roughness diminishes, which results from the increase in discharge energy that allows for much more efficient localized melting and vaporization of work piece material. This leads to the deposition of smoother craters, thus giving a general better surface finish.

WAAM-fabricated SS316L material typically has a layered microstructure with possible microscopic in-homogeneities such as fusion boundaries, interlayer porosity, and directional grain growth. Higher energy input associated with longer 'T_{on}' and increased current have made it possible to more effectively remove the irregularities and, thereby, reduces surface asperities improving the quality of the machined surface. Higher discharge current emits an even greater amount of energy per pulse and this increases the depth and consistency of material removal and contributes to smoothness. On the contrary, the extended pulse-off time (T_{off}) lengthens the duration between consecutive discharges, thereby decreasing average energy input per unit time and could probably result in non-uniform distribution of the sparks, leading to irregular material erosion and

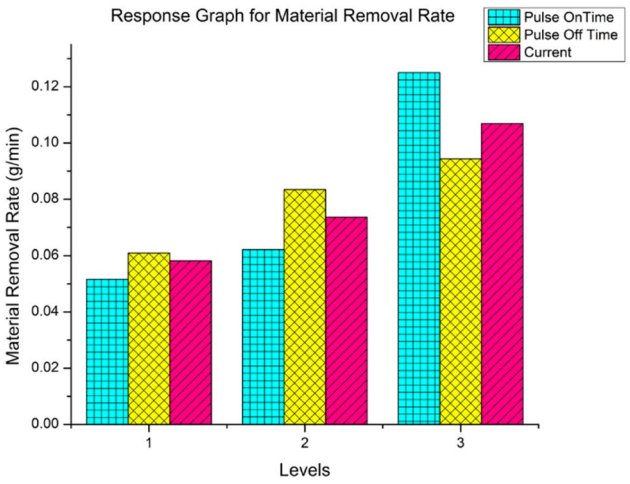

Fig. 3. Response plot for MRR.

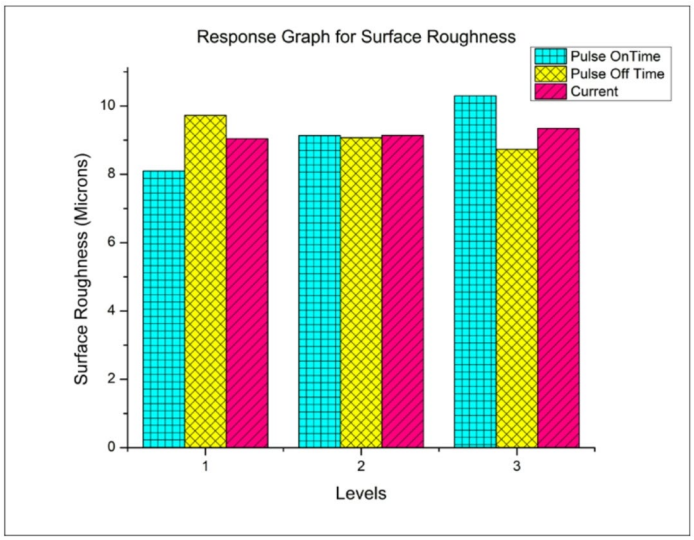

Fig. 4. Response plot for SR.

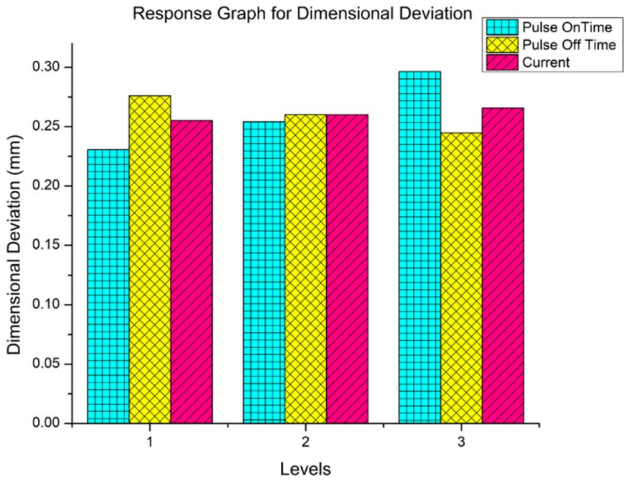

Fig. 5. Response plot for DD.

ineffective flushing of molten debris, especially on the heterogeneous and porous surfaces, like those of WAAM components, thus degrading surface quality. This means that the combination of high thermal input (T_{on} and current) and a well-controlled spark interval (T_{off}) is paramount to achieving optimal surface quality in WAAM SS316L component WEDM.

Ascendency of factors on dimensional deviation

Dimensional deviation in the WEDM machining of WAAM-fabricated SS316L was found to be strongly dependent on process parameters, as depicted in Fig. 5. Increased dimensional deviations were seen with an increase in pulse-on time (T_{on}) and applied current, while longer pulse-off times (T_{off}) helped to decrease the dimensional deviations.

Increasing 'T_{on}' prolongs the electrical discharge, putting greater thermal energy into the work piece and, therefore, into developing larger and deeper craters with consequence overcut, where the material removal beyond the intended dimension is increased. Likewise, a higher applied current increases the energy per pulse, enlarging the effective spark impact zone, further contributing to localized thermal damage, wire deflection, and irregular erosion along the cutting path. The effect is even more pronounced in WAAM-fabricated SS316L since it is fabricated in a layer-by-layer manner that causes microstructural anisotropy, residual stresses, and spatial variation in thermal conductivity, which aggravate thermal dilation and dimensional inaccuracies. Higher 'T_{off}', on the contrary, allows enough time for the dielectric to recover its insulating properties and effectively flush borne molten debris away from the spark gap, resulting in stable and uniform spark generation and comparatively lower wire vibration with no short circuiting, thus enhancing the machining precision and reducing the dimensional deviations. Hence, 'T_{on}' and current pair producing excessive thermal input and 'T_{off}'

recovering from that cooling effect shall harmoniously dictate the dimensional accuracy in WEDM of WAAM-fabricated SS316L, which warrants the careful optimization of discharge parameters for precise material removal.

Ascendency of factors on parallelism error

Evidently the resultant parallelism error in the WEDM machining of SS316L made from WAAM depended purely on the process parameters which was shown graphically in Fig. 6. Higher time in pulse-on (T_{on}) as well as higher current used increased parallelism errors. However, longer 'T_{off}' effectively reduced these errors. The major reason for parallelism error is a non-uniform removal of material, wire deflections, and thermal distortion on machined surfaces. In every electrical discharge, prolonging the time 'T_{on}' means higher heat accumulation in the work piece, leading to the formation of a zone of localized melting or uneven erosion through the thickness of the component.

This effect is most notable for WAAM SS316L due to anisotropic thermal response as well as uneven material removal because of their layered structure, directional grain orientation, and residual stresses that lead to anisotropic thermal response. Furthermore, higher current yields increased energy per pulse, further aggravating the problem of non-uniform erosion and causing deflection of the wire due to different spark force distributions, and worsening the attained dimension and geometric accuracy. On the other hand, a longer 'T_{off}' gives the time for dielectric medium to regain its insulating properties and ensures effective flushing of molten debris from the spark gap; this stabilizes the sparking process and reduces wire vibration, hence achieving greater efficiency in removing materials uniformly, thus resulting in better geometric accuracy.

The optimum parameter combination (A1B3C1) holds a kind of 'T_{on}' that is lower, a 'T_{off}' that is high, along with little current applied, therefore giving rise to the least thermal distortions and sparking stable conditions with reduced deflection from the wire itself, resulting in the lowest parallelism error. This trend highlights the importance of limiting excessive thermal input and maintaining discharge stability when aiming for high geometric precision in the WEDM machining of WAAM-fabricated components.

Ascendency of factors on perpendicularity error

WEDM machining of WAAM-fabricated SS316L showed strong dependence of the perpendicularity error on process parameters, as depicted in Fig. 7. While higher perpendicularity errors were associated with increased pulse-on time (T_{on}) and applied current, such errors reduced with increasing pulse-off time (T_{off}). The perpendicularity error arises when respective surfaces fail to maintain an identical angle between them, mainly due to the in-homogeneous removal of material by thermal distortion and wire deflection during machining.

The longer the 'T_{on}' is, the longer the time for electrical discharge runs, applying that much more thermal energy to the work piece and creating a deeper crater, or aggressively destroying the material. This process can overcut and cause lateral thermal damage to WAAM-fabricated SS316L, which is anisotropic with respect to the layers, residual stresses, and microstructural heterogeneities. These properties then magnify localized thermal expansion and deviate from the true perpendicularity.

Similarly, the applied current raises the energy per discharge, hence increasing the material removal and thermal load, but this energy in turn leads to instability in the sparking process. This enhances wire deflection and reduces angular precision along machined edges, thereby causing higher perpendicularity error. 'T_{off}' intervals on the other hand favour dielectric recovery and efficient debris removal from the spark gap, providing stabilization of the sparking process, reducing wire vibration, and uniform material erosion. This kind of controlled material removal becomes paramount in the case of WAAM-fabricated components, which suffer surface roughness, interlayer porosity, and microstructural inconsistency. Therefore, an optimum combination of lesser 'T_{on}', current, and longer 'T_{off}' time will reduce perpendicularity errors to achieve more excellent angular precision during WEDM machining of WAAM-fabricated SS316L.

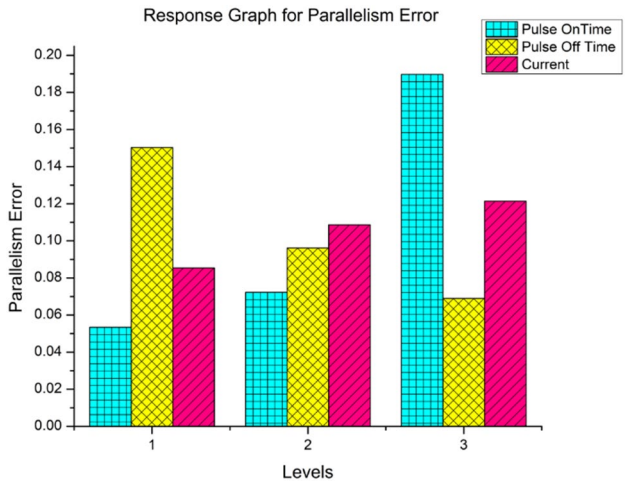

Fig. 6. Response plot for Parallelism Error.

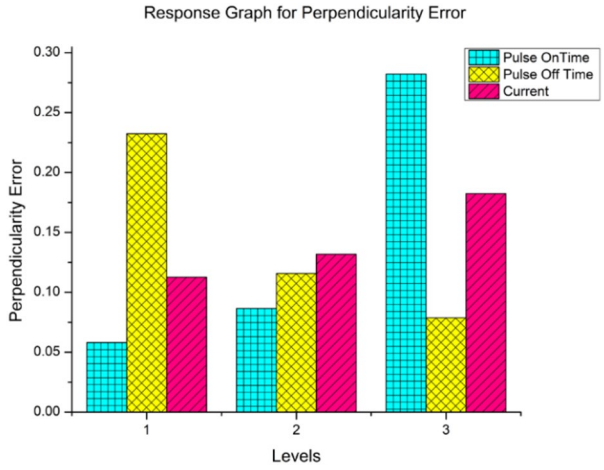

Fig. 7. Response plot for Perpendicularity Error.

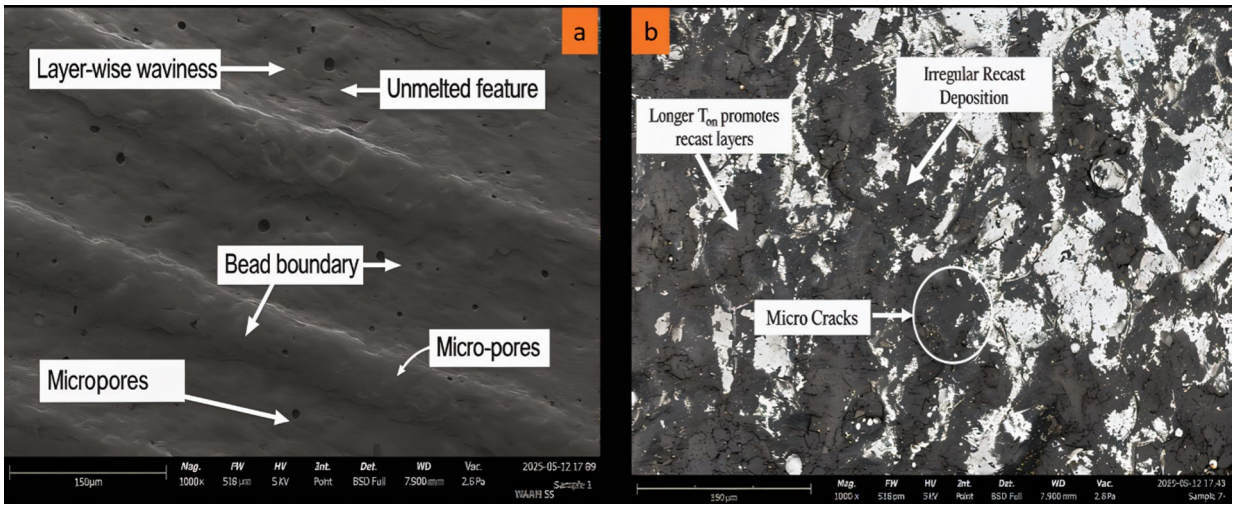

Fig. 8. SEM micrographs showing surface morphology of WAAM-fabricated SS316L after WEDM: (**a**) recast layer and micro-cracks at high magnification, (**b**) debris re-solidification and surface texture under optimized Ton = 35 µs, Toff = 10 µs, and current = 3 A conditions.

The optimal combinations of $A_1B_3C_1$ lower 'T_{on}', high 'T_{off}', and low applied current minimizes thermal stress, wire deflection, and spark-induced asymmetry, thereby reducing perpendicularity error. This trend confirms that controlled energy input and sufficient spark recovery time are crucial for achieving precise angular geometry when machining WAAM-fabricated SS316L using WEDM.

A comparative evaluation revealed that while milling and laser polishing enhance WAAM part quality, both face limitations—milling suffers from tool access, wear, and mechanical distortion, while laser polishing risks thermal distortion and microstructural alteration [1,2,48]. In contrast, optimized WEDM achieved a low surface roughness with minimal thermal impact and superior geometric precision on WAAM SS316L. This demonstrates WEDM's capability as a precise, non-contact finishing technique ideal for intricate geometries where conventional methods are constrained, aligning with prior findings on hybrid manufacturing and WAAM post-processing performance [1, 2, 48, 4].

Analysing the WEDM-processed WAAM fabricated sample

The SEM image of the WEDM-machined WAAM-fabricated stainless steel 316 L presents a surface showing recast layers, micro-cracks, and partial debris characteristic of the localized strong thermal energy and rapid cooling generated in the WEDM process as shown in Fig. 8 (a&b).

The bright contrast regions correspond to re-solidified molten material (recast layer), while darker zones represent the base substrate, showing localized micro-cracks induced by rapid quenching. Spherical to irregular particles are signs of partial reattachment of molten debris most likely due to inadequate flushing in the discharge cycle. Nevertheless, the morphology suggests that WEDM can successfully machine WAAM-fabricated components and serve as an effective post-processing tool. With optimized input parameters, WEDM

reduces recast layer formation and thermal impact significantly, thus improving surface quality and dimensional accuracy of additively manufactured stainless steel components. Overall, the SEM results reveal high promise of this hybrid manufacturing process combining the geometrical flexibility of WAAM with the finishing precision of WEDM for advanced industrial applications.

The quantitative assessment of the SEM micrographs reflected a recast layer thickness of 8–15 µm, micro-crack widths of 0.8–2.4 µm, and debris particle size of 3–12 µm, indicating their strong dependency upon pulse-on time, pulse-off time, and discharge current. In the SEM micrograph, the regions of interest have been highlighted for the distribution of recast layer formation and micro cracks. The variation of recast features is closely related to the machining parameters: longer pulse-on time (T_{on}), increasing thermal load, produces thicker and greater uneven recast layers, and a shorter pulse-off time (T_{off}) inhibits dielectric recovery, thereby leading to unstable discharges and irregular recast deposition; maximum intensity of discharge current leads to localized melting in a more controlled manner that thickens re-solidified regions on existing surface defects. All of these observations illustrate strong interdependencies between the morphology of recast layer and 'T_{on},' 'T_{off},' and current.

Evolution of ANFIS structure for WEDM of WAAM fabricated SS material

The MATLAB toolbox was used to build and refine ANFIS models that forecast the proposed GRG. In this work, the ANFIS model was built with three input and one output. The model was trained using experimental data and then tested to predict target performance metrics. The training configurations and parameters adopted in this exploration are depicted in Table 3.

The ANFIS model was created using 'trimf' (triangular membership function) and operates on a set of 27 rules generated automatically through processing the input data given to the system. A comparative approach initiated under the framework Multi-Criteria Decision Making (MCDM) is the method called Grey Relational Analysis (GRA) to assess the Grey Relational Grade (GRG) values. The ANFIS editor corresponding to the developed model is shown in Fig. 9. The trained model is now being used to predict the multi-performance index called ANFIS-GRG.

Interpretation on outcomes of ANFIS analysis for GRG

The ANFIS surface plots derived from the WEDM experimentation on WAAM-fabricated stainless steel reveal the complex nonlinear relationships between process responses and their combined effect on the predicted GRG as depicted in Fig. 10 (a–d).

The model effectively captures the interactive influence of input parameters such as MRR, SR, DD, Parallelism Error (PRL_ERR), and Perpendicularity Error (PERP_ERR). An overall increase in GRG is observed with higher MRR and improved surface quality, while dimensional accuracy parameters like DD, PRL_ERR, and PERP_ERR show a significant impact on performance, indicating their sensitivity and importance. The plots definitely prove that maximum productivity and minimum geometrical deviations shall produce a workable result toward establishing the strength and predictive capability of the evolved ANFIS model for WEDM of WAAM-fabricated stainless steel.

The surface plot in Fig. 11(a) depicts the interaction between GRC_DD and GRC_PERP_ERR (Perpendicularity Error) in predicting the ANFIS-based Grey Relational Grade (GRG). It is apparent that GRG presents a steep change with change in both parameters, indicating that the model is very sensitive to even slight changes in dimensional and geometrical accuracy.

Higher GRG is attained at lower values of both DD and PERP_ERR, indicating that tight tolerances in dimensional and perpendicular accuracy are essential for enhancing the performance of machining. In Fig. 11 (b), the interaction between GRC_DD and GRC_PRL_ERR is illustrated. The surface indicates a strong influence of profile accuracy on the GRG, with performance improving significantly when both profile error and dimensional deviation are minimized. The steep rise in GRG over a narrow band of values suggests a sharp threshold for optimal machining conditions, reinforcing the need for precise control of these error metrics during the WEDM process.

The surface plot in Fig. 12(a) illustrates the interaction between GRC_SR (Surface Roughness) and GRC_DD (Dimensional Deviation) on the ANFIS-predicted GRG. It is evident that a higher GRG is achieved when both surface roughness and dimensional deviation are minimized, indicating their significant contribution to overall machining performance. In Fig. 12(b), the correlation amongst GRC_SR and GRC_PERP_ERR (Perpendicularity Error) is depicted. The GRG increases with decreasing perpendicularity error, especially in regions of moderate surface roughness. This highlights the combined importance of geometric precision and surface integrity. Figure 12(c) presents the interaction of GRC_SR with GRC_PRL_ERR (Profile Error).

No. of membership functions	3 3 3 3 3
Input 'mf' opted	trimf
Output 'mf' opted	constant
Optimizing Approach	Back propagation
Tolerance of Error level	0
Epochs numbers opted	500

Table 3. ANFIS Training variables for WEDM of HMMC.

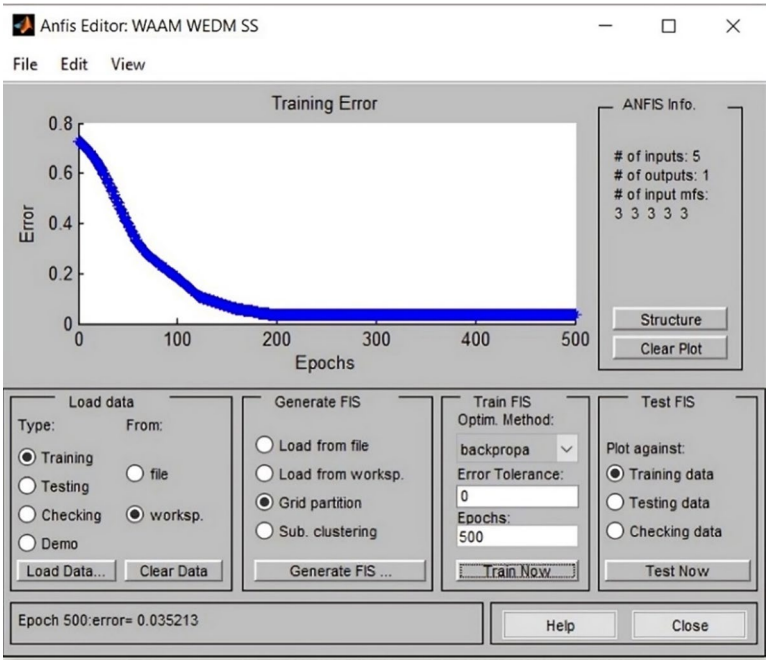

Fig. 9. ANFIS Editor.

The GRG sharply rises as both surface roughness and profile error decrease, emphasizing that profile accuracy significantly influences the overall performance when surface finish is within acceptable limits.

In Fig. 12(d), the combined effect of GRC_PERP_ERR and GRC_PRL_ERR on GRG is shown. A complex, non-linear surface is observed, with GRG peaking when both error metrics are at their lowest, revealing a critical zone where machining precision in geometry directly enhances the performance index. Surface plots portray that minimizing surface roughness, dimensional, profile, and perpendicularity errors is critical to chambering the work piece into an optimal condition. The successful interdependence captured by the ANFIS model guarantees that it is a valid tool for multi-performance prediction in WEDM of WAAM-fabricated stainless steel.

Analysing performance of evolved ANFIS model

The discrepancy between the experimentation data and the envisaged data developed by the evolved model is referred to as the error. To assess the model, numerous statistical measures are computed, containing Mean Absolute Percentage Error (MAPE), Root Mean Square Error (RMSE), and the coefficient of correlation. These metrics are calculated using the Eq. (1) to (3).

$$Mean\ Absolute\ Percentage\ Error\ \mathrm{MAPE}\,(\%) = \frac{1}{\mathrm{n}}\sum\nolimits_{\mathrm{i}=1}^{\mathrm{n}} \frac{\mathrm{E_V} - \mathrm{P_V}}{\mathrm{E_V}} * 100 \tag{1}$$

$$Root\ Mean\ Square\ Error\ \mathrm{RMSE} = \sqrt{\frac{1}{\mathrm{n}}\sum\nolimits_{\mathrm{i}=1}^{\mathrm{n}} (\mathrm{E_v} - \mathrm{P_v})^2} \tag{2}$$

$$Correlation\ coefficient\ \ \mathrm{R}^2 = 1 - \frac{\sum\nolimits_{\mathrm{m}=1}^{\mathrm{n}} (\mathrm{Pv} - \mathrm{Ev})^2}{\sum\nolimits_{\mathrm{m}=1}^{\mathrm{n}} (\mathrm{Ev})^2} \tag{3}$$

Where,

'E_V' – experimental values.

'P_V' - forecasted values.

'n' - no. of trials.

The results of the ANFIS model for the WEDM of WAAM-fabricated stainless steel (SS) were analyzed and compared with the corresponding experimental data. A strong correlation has been observed between the actual and the predicted results that shows the reliability of the model in consideration. The performance was assessed on the basis of statistical parameters according to Eq. (1) to (3), with detailed values presented in Table 4. The RMSE and MAE are shown in Fig. 13, while Fig. 14 displays the MAPE and correlation coefficient, thereby supporting the predictive capability of the model.

ANOVA on performance measures

The ANOVA analysis has been performed to reveal the significance of independent variables on opted performance measures and it is represented in Table 5. The outcomes of the ANOVA analysis shows that, among the parameters affecting essentially all machining responses, pulse-on time (T_{on}) is the most dominant factor. Its

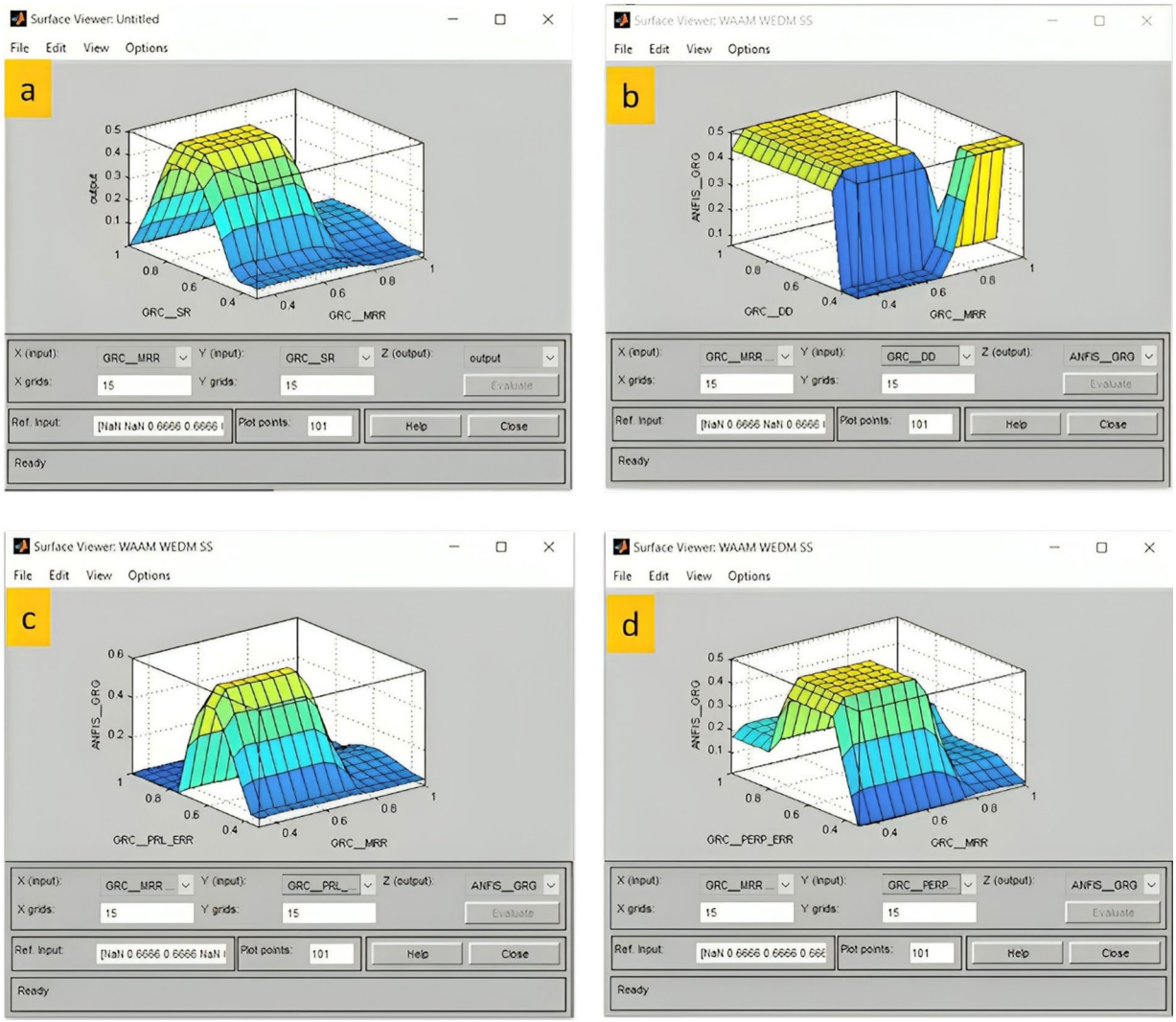

Fig. 10. (**a**) Surface plot for ANFIS-GRG vs. GRC of MRR and SR (**b**) Surface plot for ANFIS-GRG vs. GRC of MRR and GRC of DD (**c**) Surface plot for ANFIS-GRG vs. GRC of MRR and GRC of PRL Err (**d**) Surface plot for ANFIS-GRG vs. GRC of MRR and GRC of PERP Err.

effect on MRR (Material Removal Rate), dimensional deviation, and GD&T errors is quite strong due to its direct influence on both discharge energy and crater morphology, which in turn control material erosion and thermal distortion. Pulse-off time (T_{off}) also exerts notable influence, especially in the control of surface roughness and geometric precision, since a proper off time ensures dielectric recovery, stable discharge conditions, and efficient removal of debris. On the other hand, the current significantly affects MRR and surface roughness by increasing energy per spark of discharge, although its influence on dimensional and geometric errors is quite limited. In general, the ANOVA defines 'T_{on}' and 'T_{off}' as the necessary process variables for precision and consistency in WEDM of WAAM-fabricated SS316L, while current is mainly responsible for productivity and surface quality.

Conclusions

The exploratory analysis discusses the experimental assessment of WEDM conducted on WAAM-fabricated stainless steel (SS316L). An intelligent decision-making system based on hybrid ANFIS was developed to conceive the required multi-performance index. Some major findings of this exploration include:

- The integration of WAAM for near-net-shape fabrication and WEDM for precision finishing proved effective in improving surface quality, dimensional accuracy, and geometric tolerance of SS316L components.
- The stainless steel samples that were fabricated using WAAM were subjected to the WEDM process. It was found that the critical process variables, pulse length, and peak current, directly affected performance metrics such as MRR, SR, DD and GD&T errors.
- Pulse-on time (T_{on}) was confirmed as the most influential parameter affecting MRR, dimensional deviation, and GD&T errors, while pulse-off time (T_{off}) strongly influenced surface roughness and geometric stability.

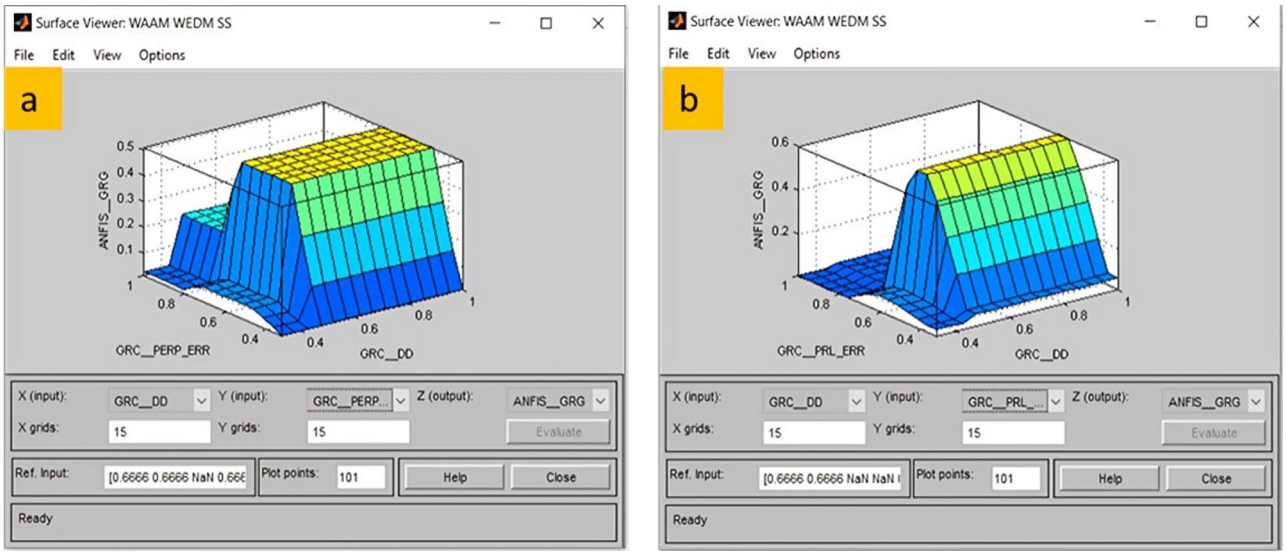

Fig. 11. (**a**) Surface plot for ANFIS-GRG vs. GRC of DD and PERP Err. (**b**) Surface plot for ANFIS-GRG vs. GRC of DD and PRL Err.

- The combined Taguchi–GRA–ANFIS framework provided a robust multi-objective optimization and predictive tool, with very high accuracy (R^2 = 0.9985, MAPE = 2.19%), confirming its suitability for modelling nonlinear machining interactions.
- The predictions made by an ANFIS model were based on experimental GRG values to calculate the overall effectiveness of the WEDM method. The predictive GRG value of 0.8756 was very close to being validated experimentally and shows the model's robustness and ability for generalization.
- The ANFIS model also achieved the very high correlation coefficient of 0.9985, implying high predictive accuracy and strong association with experimental details. Thus, the results put further evidence on the reliability and applicability of the model in predicting multi-performance outcomes in WAAM manufactured stainless steel parts on WEDM.
- The demonstrated WAAM–WEDM hybrid strategy shows strong scalability potential for aerospace, biomedical, and energy applications, where large, complex, and precision-critical components are required.
- The present work is limited to SS316L, without in-situ monitoring or direct recast layer quantification, which constrains microstructural insights and generalization across materials.
- Real-time adaptive WAAM–WEDM integration, supported by AI-driven sensing and control, along with extension to multi-material and functionally graded systems, offers significant opportunities for industrial deployment.
- Future research may focus on developing a real-time AI-driven integration of the WAAM–WEDM hybrid system to further enhance process accuracy and adaptability. Key sensing parameters such as spark gap voltage, discharge current, and pulse frequency (in WEDM), along with arc voltage, current, and melt-pool temperature (in WAAM), can provide valuable feedback for closed-loop control. Advanced algorithms including Model Predictive Control (MPC), Adaptive Neuro-Fuzzy Inference System (ANFIS), fuzzy logic, and reinforcement learning can be utilized to intelligently regulate parameters like pulse on/off time, wire feed rate, and arc current. Such an approach would enable autonomous correction of deviations, ensuring improved dimensional accuracy, reduced surface errors, and enhanced overall process stability in future WAAM–WEDM hybrid manufacturing systems.

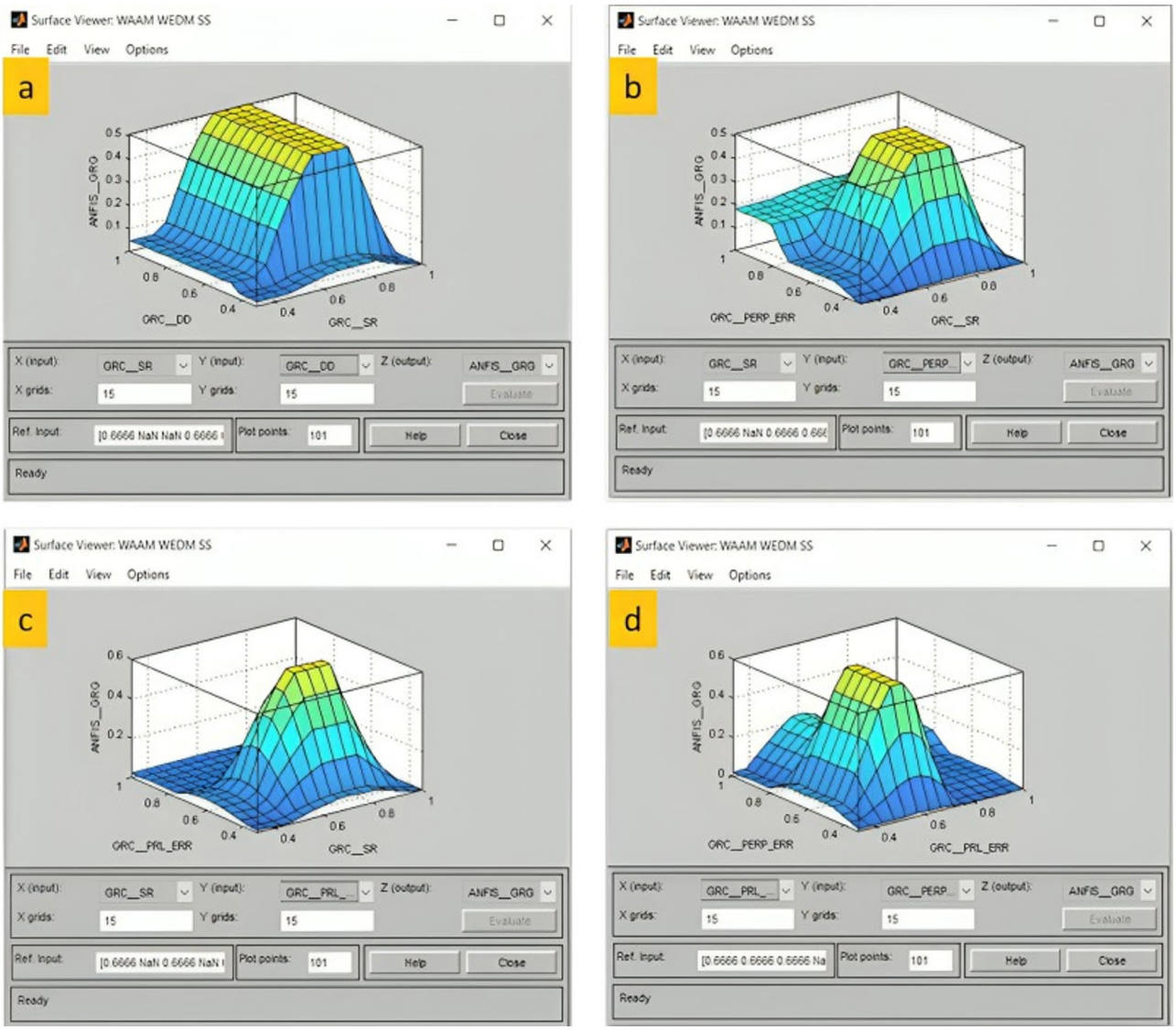

Fig. 12. (**a**) Surface plot for ANFIS-GRG vs. GRC of SR and GRC of DD (**b**) Surface plot for ANFIS-GRG vs. GRC of SR and GRC of PERP Err (**c**) Surface plot for ANFIS-GRG vs. GRC of SR and GRC of PRL Error (**d**) Surface plot for ANFIS-GRG vs. GRC of PERP Err and GRC of PRL Err.

Model - ANFIS	
Errors/Metrics	**Error Values**
MAPE	2.192
RMSE	0.0274
MAE	0.0219
Correlation Coefficient	0.9985

Table 4. Performance Metrics of ANFIS model.

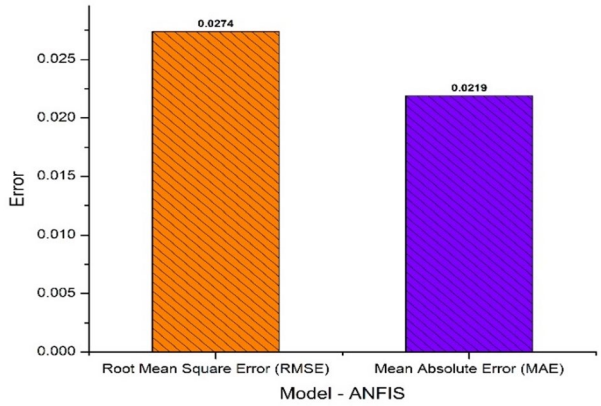

Fig. 13. Performance analysis of evolved ANFIS model.

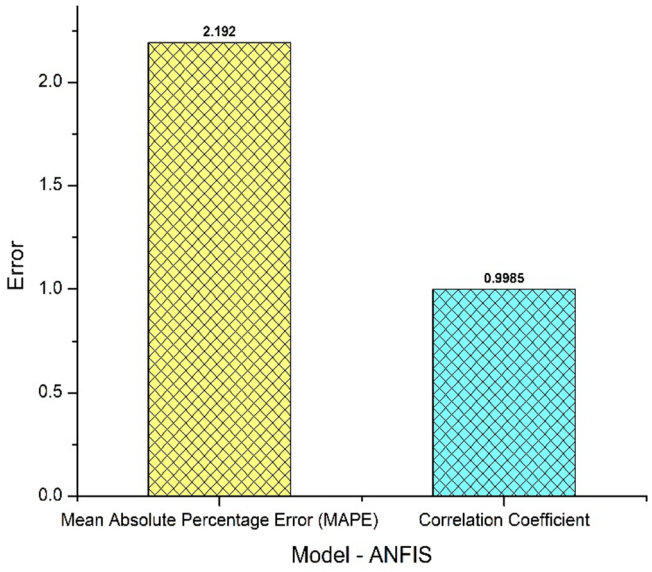

Fig. 14. Error Analysis of ANFIS model.

Source	DF	Seq SS	Adj SS	Adj MS	F	P
Material Removal Rate (g/min)						
T_{on} (µs)	2	0.028394	0.028394	0.014197	12.91	0
T_{off} (µs)	2	0.005209	0.005209	0.002605	2.37	0.119
Current (A)	2	0.011163	0.011163	0.005581	5.08	0.016
Error	20	0.021993	0.021993	0.0011		
Total	26	0.066759				
Surface Roughness (Microns)						
T_{on} (µs)	2	4.0466	4.0466	2.0233	20.41	0
T_{off} (µs)	2	18.849	18.849	9.4245	95.05	0
Current (A)	2	2.6107	2.6107	1.3054	13.17	0
Error	20	1.9831	1.9831	0.0992		
Total	26	27.4894				
Dimensional Deviation (mm)						
T_{on} (µs)	2	0.02007	0.02007	0.010035	99.33	0
T_{off} (µs)	2	0.004415	0.004415	0.002208	21.85	0
Current (A)	2	0.0005	0.0005	0.00025	2.47	0.11
Error	20	0.002021	0.002021	0.000101		
Total	26	0.027006				
Parallelism Error						
T_{on} (µs)	2	0.098152	0.098152	0.049076	14.68	0
T_{off} (µs)	2	0.030863	0.030863	0.015432	4.62	0.022
Current (A)	2	0.005981	0.005981	0.002991	0.89	0.425
Error	20	0.066861	0.066861	0.003343		
Total	26	0.201858				
Perpendicularity Error						
T_{on} (µs)	2	0.26794	0.26794	0.13397	10.72	0.001
T_{off} (µs)	2	0.11587	0.11587	0.05793	4.63	0.022
Current (A)	2	0.02335	0.02335	0.01167	0.93	0.41
Error	20	0.25004	0.25004	0.0125		
Total	26	0.65719				

Table 5. ANOVA Outcomes on performance metrics.

Data availability

The necessary data used in the manuscript are already present.

Received: 14 August 2025; Accepted: 23 March 2026
Published online: 26 March 2026

References

1. Wu, B. et al. A review of the wire arc additive manufacturing of metals: properties, defects and quality improvement. *J. Manuf. Process.* **35**, 127–139. https://doi.org/10.1016/j.jmapro.2018.08.001 (2018).
2. Dávila, J. L., Neto, P. I., Noritomi, P. Y., Coelho, R. T. & da Silva, J. V. L. Hybrid manufacturing: a review of the synergy between directed energy deposition and subtractive processes. *Int. J. Adv. Manuf. Technol.* **110**, 3377–3390. https://doi.org/10.1007/s00170-020-06062-7 (2020).
3. Wang, Z., Zhang, Y., Orquera, M., Millet, D. & Bernard, A. A new hybrid generative design method for functional & lightweight structure generation in additive manufacturing. *Procedia CIRP.* **119**, 66–71. https://doi.org/10.1016/j.procir.2023.02.127 (2023).
4. Sasikumar, C. & Oyyaravelu, R. Mechanical properties and microstructure of SS316L created by WAAM based on GMAW. *Mater. Today Commun.* **38**, 107807. https://doi.org/10.1016/j.mtcomm.2023.107807 (2024).
5. Manikandan, N., Binoj, J. S., Thejasree, P., Sasikala, P. & Anusha, P. Application of Taguchi method on wire electrical discharge machining of Inconel 625. *Mater. Today: Proc.* **39**, 121–125 (2021).
6. Manikandan, N., Binoj, J. S., Krishnamachary, P. C. & Thejasree, P. & Arul Kirubakaran, D. Predictive models for wire spark erosion machining of AA 7075 alloy using multiple regression analysis. In *Advances in Industrial Automation and Smart Manufacturing: Select Proceedings of ICAIASM 2019*, 429–438Springer, Singapore, (2020).
7. Kruth, J. P., Leu, M. C. & Nakagawa, T. Progress in additive manufacturing and rapid prototyping. *CIRP Ann. Manuf. Technol.* **47**, 525–540. https://doi.org/10.1016/s0007-8506(07)63240-5 (1998).
8. Edwards, K. L. Rapid manufacturing — the technologies and applications of rapid prototyping and rapid tooling. *Mater. Eng.* **23**, 347–348. https://doi.org/10.1016/s0261-3069(01)00077-2 (2002).
9. Gogineni, A., Kale, R. V., Roy, S., Modi, P. & Kumar, P. Spatial Assessment of Snow Cover Patterns in the Sutlej River Basin Using Machine Learning Approaches and Remote Sensing Data. *Physics Chem. Earth Parts A/B/C*, 103996. (2025).
10. Achillas, C., Tzetzis, D. & Raimondo, M. O. Alternative production strategies based on the comparison of additive and traditional manufacturing technologies. *Int. J. Prod. Res.* **55**, 3497–3509. https://doi.org/10.1080/00207543.2017.1282645 (2017).

11. Steenhuis, H. J. & Pretorius, L. Consumer additive manufacturing or 3D printing adoption: an exploratory study. *J. Manuf. Technol. Manag.* **27**, 990–1012. https://doi.org/10.1108/jmtm-01-2016-0002 (2016).
12. Mani, M., Lane, B. M., Donmez, M. A., Feng, S. C. & Moylan, S. P. A review on measurement science needs for real-time control of additive manufacturing metal powder bed fusion processes. *Int. J. Prod. Res.* **55**, 1400–1418. https://doi.org/10.1080/00207543.2016.1223378 (2017).
13. Srivastava, M. & Rathee, S. Additive manufacturing: recent trends, applications and future outlooks. *Prog Addit. Manuf.* **7**, 261–287. https://doi.org/10.1007/s40964-021-00229-8 (2022).
14. Khoo, Z. X. et al. Y. 3D printing of smart materials: a review on recent progresses in 4D printing. *Virtual Phys. Prototyp.* **10**, 103–122. https://doi.org/10.1080/17452759.2015.1097054 (2015).
15. Pei, E. 4D printing: dawn of an emerging technology cycle. *Assem Autom.* **34**, 310–314. https://doi.org/10.1108/aa-07-2014-062 (2014).
16. Tibbits 4D printing: multi-material shape change. *Archit. Des.* **84**, 116–121. https://doi.org/10.1002/ad.1710 (2014).
17. Gogineni, A., Sharma, S., Roy, S. & Kumar, P. Long-Term drought analysis and forecasting using hybrid wavelet Denoise random forest models with SPI, Z-Score, and China Z-Index. *Arabian J. Sci. Engineering*, 1–29. (2025).
18. Somsole, L. N. et al. Experimental investigation and optimization of epoxy composites reinforced with jute fiber and alumina using the Jaya ANFIS approach. *Sci. Rep.* **15** (1), 30462 (2025).
19. Li, F., Zhang, W., Kooi, B. J. & Pei, Y. Eutectic aluminum alloys fabricated by additive manufacturing: a comprehensive review. *J. Mater. Sci. Technol.* **250**, 123–164. https://doi.org/10.1016/j.jmst.2025.06.016 (2026).
20. Natarajan, M. et al. Investigational analysis on wire electrical discharge machining of aluminium based composites by Taguchi's method. SAE Tech. Pap. -28-0075 (2023). (2023).
21. Natarajan, M. et al. Evolution of regression and neural network models on wire electrical discharge machining of nickel-based superalloy. SAE Tech. Pap. -28-0078 (2023). (2023).
22. Natarajan, M., Pasupuleti, T., Katta, L. N., Somsole, L. N. & Kiruthika, J. Application of Taguchi approach on wire electrical discharge machining of SS304 for automotive applications. SAE Tech. Pap. -28-0151 (2023). (2023).
23. Gebhardt, A. Materials, design, and quality aspects for additive manufacturing. In *Understanding Additive Manufacturing*, 129–149 (Carl Hanser Verlag, München, (2011).
24. Manikandan, N., Binoj, J. S., Varaprasad, K. C., Thejasree, P. & Raju, R. Investigations on wire electrical discharge machining of nickel-based superalloy using Taguchi's approach. In *Advances in Industrial Automation and Smart Manufacturing: Select Proceedings of ICAIASM 2019*, 267–274Springer, Singapore, (2020).
25. ASTM F42 Committee. *Terminology for Additive Manufacturing – General Principles – Terminology* (ASTM International, 2017).
26. Ahn, D. G. Directed energy deposition (DED) process: state of the art. *Int. J. Precis Eng. Manuf. -Green Technol.* **8**, 703–742. https://doi.org/10.1007/s40684-020-00302-7 (2021).
27. Binoj, J. S. et al. Machinability studies on wire electrical discharge machining of nickel alloys using multiple regression analysis. *Mater. Today: Proc.* **39**, 155–159 (2021).
28. Natarajan, M., Pasupuleti, T., Silambarasan, R. & Katta, L. N. Development of prediction models for spark erosion machining of SS304 using regression analysis. SAE Tech. Pap. -28-0339 (2022). (2022).
29. Singh, A., Kapil, S. & Das, M. A comprehensive review of the methods and mechanisms for powder feedstock handling in directed energy deposition. *Addit. Manuf.* **35**, 101388. https://doi.org/10.1016/j.addma.2020.101388 (2020).
30. Manikandan, N., Thejasree, P., Reddy, D. R. & Kumar, P. P. Development of regression model and optimization of process parameters for wire electrical discharge of SAE 1010 steel using Taguchi grey approach. *J. Phys. : Conf. Ser.* **2837**, 012084 (2024).
31. Zhang, J. *Additive manufacturing: materials, processes, quantifications and applications* (Butterworth-Heinemann, 2018).
32. Tang, Z. J. et al. H.-C. A review on in situ monitoring technology for directed energy deposition of metals. *Int. J. Adv. Manuf. Technol.* **108**, 3437–3463. https://doi.org/10.1007/s00170-020-05569-3 (2020).
33. Zhang, D., Lim, W. Y. S., Duran, S. S. F., Loh, X. J. & Suwardi, A. Additive manufacturing of thermoelectrics: emerging trends and outlook. *ACS Energy Lett.* **7**, 720–735. https://doi.org/10.1021/acsenergylett.1c02553 (2022).
34. Pasupuleti, T., Natarajan, M., Katta, L. N. & Naidu, B. V. V. Microstructure and mechanical behaviour of dissimilar laser welded joints for automobile applications. *SAE Int. J. Adv. Curr. Pract. Mobil.* **5**, 1592–1595 (2022).
35. Raju, R. et al. Optimization and performance evaluation of PLA polymer material in situ carbon particles on structural properties. *Mater. Today: Proc.* 39, 223–229 (2021).
36. Seow, C. E. et al. Wire + arc additively manufactured Inconel 718: effect of post-deposition heat treatments on microstructure and tensile properties. *Mater. Des.* **183**, 108157. https://doi.org/10.1016/j.matdes.2019.108157 (2019).
37. Fu, Y. et al. Optimization of shape and performance for wire and arc additive manufacturing with in-situ rolling of Ti–6Al–4V ELI alloy. *J. Mater. Res. Technol.* **35**, 4833–4847. https://doi.org/10.1016/j.jmrt.2025.02.068 (2025).
38. Kumar, L., Goyal, A. & Pathak, V. K. Prediction and optimization of WEDM parameters for machining of NiTi-shape memory alloy using ANFIS-PSO approach. *Discov Appl. Sci.* **7**, 1–. https://doi.org/10.1007/s42452-025-06663-5 (2025).
39. Chauhan, P., Vaghasia, V., Chaudhari, R. & Vora, J. Experimental investigations on the fabrication of low alloy steels using wire arc additive method. *Eur. Proc. Sci. Technol. Eng. Math.* **28**, 484–491. https://doi.org/10.55549/epstem.1523859 (2024).
40. Thejasree, P. & Krishnamachary, P. C. Weldability investigations on laser welding of Inconel 718 plates using Taguchi approach. In *Recent Advances in Materials and Modern Manufacturing: Select Proceedings of ICAMMM 2021*, 245–254Springer, Singapore, (2022).
41. Zaman, U. K., Rivette, M., Siadat, A. & Mousavi, S. M. Integrated product-process design: material and manufacturing process selection for additive manufacturing using multi-criteria decision making. *Robot Comput. Integr. Manuf.* **51**, 169–180. https://doi.org/10.1016/j.rcim.2017.12.005 (2018).
42. Sarathchandra, D. T., Davidson, M. J. & Visvanathan, G. Parameters effect on SS304 beads deposited by wire arc additive manufacturing. *Mater. Manuf. Process.* **35**, 852–858. https://doi.org/10.1080/10426914.2020.1743852 (2020).
43. Grzesik, W. Hybrid additive and subtractive manufacturing processes and systems: a review. *J. Mach. Eng.* **18**, 5–24. https://doi.org/10.5604/01.3001.0012.7629 (2018).
44. Antunes, F. et al. Fatigue crack growth in maraging steel obtained by selective laser melting. *Appl. Sci.* **9**, 4412. https://doi.org/10.3390/app9204412 (2019).
45. Singh, S., Sharma, S. K. & Rathod, D. W. A review on process planning strategies and challenges of WAAM. *Mater. Today*. **47**, 6564–6575. https://doi.org/10.1016/j.matpr.2021.02.632 (2021).
46. Vishwanatha, Rao, R. N. et al. Effects of arc current and travel speed on the processing of stainless steel via wire arc additive manufacturing (WAAM) process. *J. Adhes. Sci. Technol.* **38**, 2222–2239. https://doi.org/10.1080/01694243.2023.2289770 (2024).
47. Manikandan, N. et al. Integration of hybrid grey based ANFIS tool for enhanced laser beam welding of nickel alloy using computational modelling. *Int J. Interact. Des. Manuf* 1–12 (2024).
48. Asad, M., Sana, M., Farooq, M. U. & Tlija, M. Producing micro impressions on Al6061 under alumina-mixed deionized water as dielectric during electric discharge machining. *J. Micromech Microeng.* **35**, 035011. https://doi.org/10.1088/1361-6439/adb044 (2025).
49. Sana, M., Asad, M., Farooq, M. U., Tlija, M. & Haber, R. Sustainability metrics targeted optimization and electric discharge process modelling by neural networks. *Sci. Rep.* **15**, 3375. https://doi.org/10.1038/s41598-024-78883-5 (2025).
50. Hannan, A. et al. Machining performance, economic and environmental analyses and multi-criteria optimization of electric discharge machining for SS310 alloy. *Sci. Rep.* **14**, 28930. https://doi.org/10.1038/s41598-024-79338-7 (2024).

51. Hurairah, M. A., Sana, M., Farooq, M. U. & Anwar, S. Genetic algorithm-based optimization of artificial neural network of process parameters and characterization of machining errors in graphene mixed dielectric. *Arab. J. Sci. Eng.* https://doi.org/10.1007/s13369-024-09029-y (2024).
52. Farooq, M. U., Ali, M. A., Anwar, S. & Bhatti, H. A. Process parameters optimization and performance analysis of micro-complex geometry machining on Ti6Al4V. *Int. J. Interact. Des. Manuf.* **18**, 4573–4593. https://doi.org/10.1007/s12008-023-01711-z (2024).
53. Kokare, S. et al. Wire arc additive manufacturing of a high-strength low-alloy steel part: environmental impacts, costs, and mechanical properties. *Int. J. Adv. Manuf. Technol.* **134**, 453–475 (2024).
54. Pasupuleti, T., Natarajan, M. & Silambarasan, R. Development of regression models for laser beam welding of Inconel 718 alloy thin sheets. SAE Tech. Pap. -28-0340 (2022). (2022).
55. Li, S. H., Kumar, P., Chandra, S. & Ramamurty, U. Directed energy deposition of metals: processing, microstructures, and mechanical properties. *Int. Mater. Rev.* **68**, 605–647. https://doi.org/10.1080/09506608.2022.2097411 (2023).
56. Lim, J. S., Oh, W. J., Lee, C. M. & Kim, D. H. Selection of effective manufacturing conditions for directed energy deposition process using machine learning methods. *Sci. Rep.* **11**, 24169. https://doi.org/10.1038/s41598-021-03622-z (2021).

Acknowledgements
The authors gratefully thank the authors' respective institutions for their strong support of this study.

Author contributions
P. Thejasree: Conceptualization, Data curation, Formal analysis, Investigation, Writing - original draft. N. Manikandan: Writing – original draft, Writing – review & editing. Siva Marimuthu: Supervision, Validation, Visualization, Investigation, Review & editing. Rajadurai Murugesan: Writing – original draft, Writing – review & editing. D. Palanisamy: Writing – original draft, Writing – review & editing. Mukesh Kumar: Writing – original draft, Writing – review & editing. Arun Kumar: Writing – review & editing. Regasa Yadeta Sembeta: Project administration, Writing – original draft, Writing – review and editing.

Funding
This research received no external funding.

Declarations

Competing interest
The authors declare no competing interests.

Ethical approval
This study did not involve human participants or animals; no ethical approval was required. All research procedures adhered to relevant ethical guidelines and best practices for non-human and non-animal research.

Consent for publication
The authors declare that this manuscript is original, has not been published before and is not currently being considered for publication elsewhere. The authors confirm that the manuscript has been read and approved by all named authors and that no other persons have satisfied the criteria for authorship but are not listed. The authors further confirm that all have approved the order of authors listed in the manuscript of us. The authors understand that the corresponding author is the sole contact for the Editorial process. The corresponding author is responsible for communicating with the other authors about progress, submissions of revisions and final approval of proofs. No additional information is available for this paper.

Additional information
Correspondence and requests for materials should be addressed to R.Y.S.

Reprints and permissions information is available at www.nature.com/reprints.

Publisher's note Springer Nature remains neutral with regard to jurisdictional claims in published maps and institutional affiliations.